Tao, Z., Li, A., and Fischer, K.M., 2021, Hotspot signatures at the North American passive margin: Geology, v. 49, https://doi.org/10.1130/G47994.1

SUPPLEMENTAL MATERIAL

Methods

We inverted the isotropic 1-D Vsv and Vsh models from the obtained Rayleigh wave and Love wave phase velocities at each node using the model AK135 as the starting model (Kennett et al., 1995). A stochastic generalized linear inversion method was used with smoothing between adjacent model parameters and constraints to the initial model. The controlling parameters were tested so that the resulting velocity model varies smoothly with depth and stays close to the initial model at depths >260 km, where the data do not have much sensitivity. Partial derivatives of phase velocities with respect to Vsv and Vsh are calculated using Saito's method (1988).

For anisotropic inversions, we followed the technique of Li et al. (2016) and solved two model parameters Vsv and ξ in each layer. Other anisotropic parameters are calculated using linear relations with ξ. We built the initial anisotropic models based on the isotropic Vsv and Vsh velocities. The a priori standard errors of model parameters are set for damping the solutions. We found the resulting anisotropic model that fits the data best is very close to the initial anisotropic model, indicating that the Vsv and Vsh models from isotropic inversions are good approximations of the anisotropic models. Our 3-D anisotropic models of Vsv and ξ are developed by collecting the 1-D models at all map points.

Figures

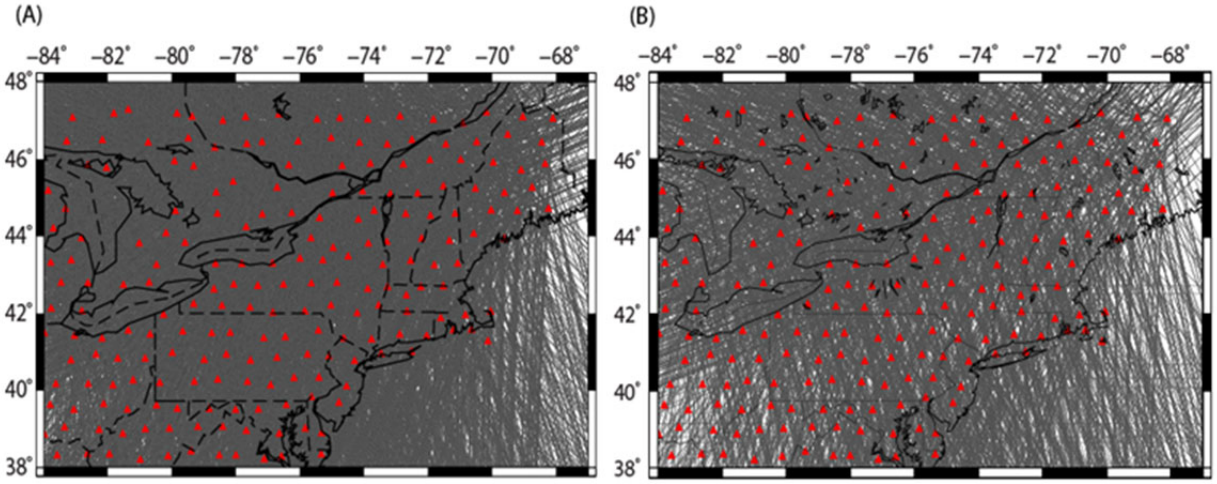

Figure S1. Great circle ray paths of the data at period 50 s for Rayleigh wave (A) and Love wave (B), respectively. Red triangles are for the TA stations used in this study. Crossing ray paths also appear outside the array near the coast, allowing good model resolution at the continental margin.

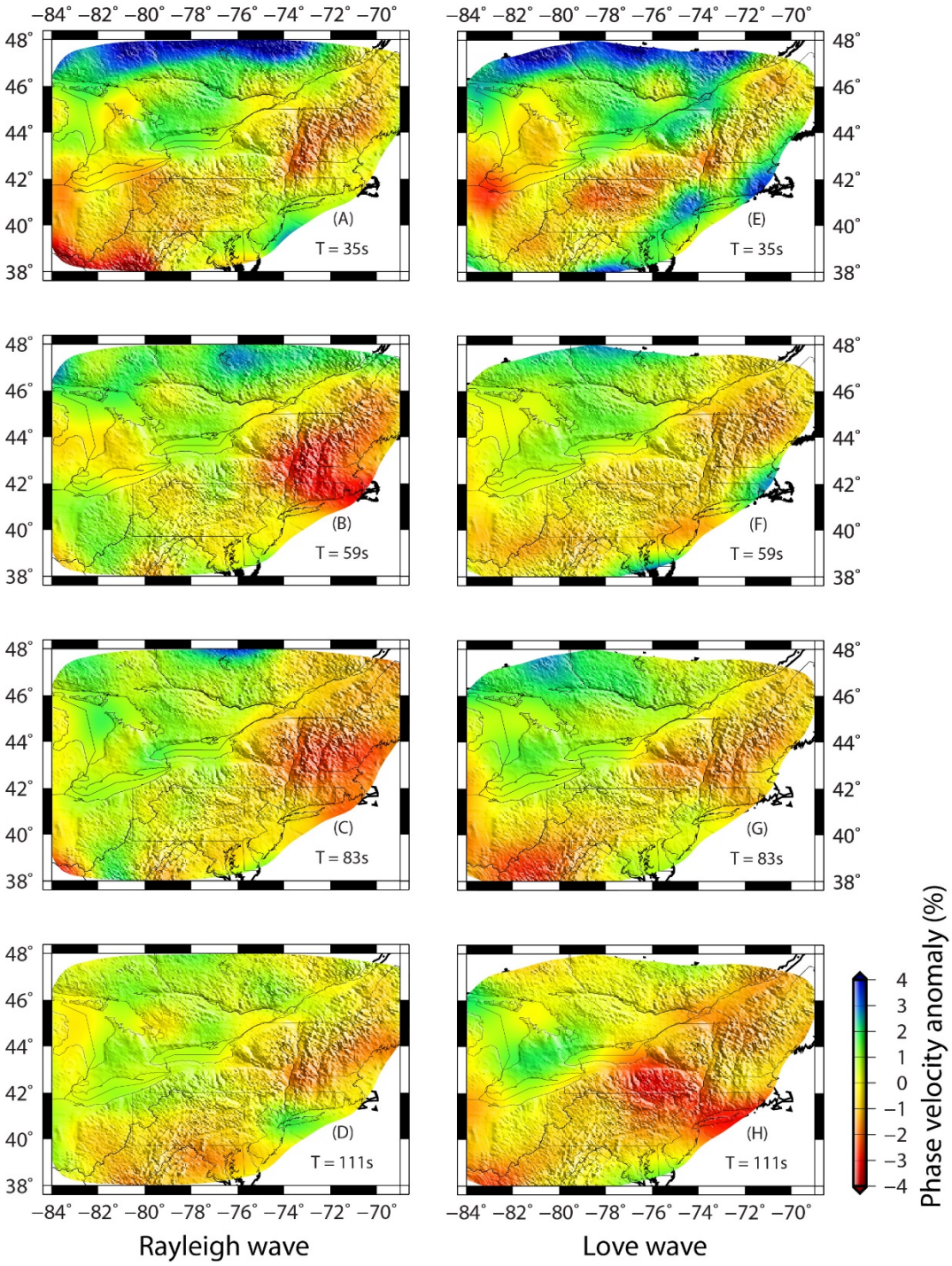

Figure S2. Maps of phase velocity perturbations for Rayleigh wave (A, B, C, and D) and Love wave (E, F, G, and H) at period 35 s, 59 s, 83 s, and 111 s. The perturbations are calculated with respect to the average values of each period.

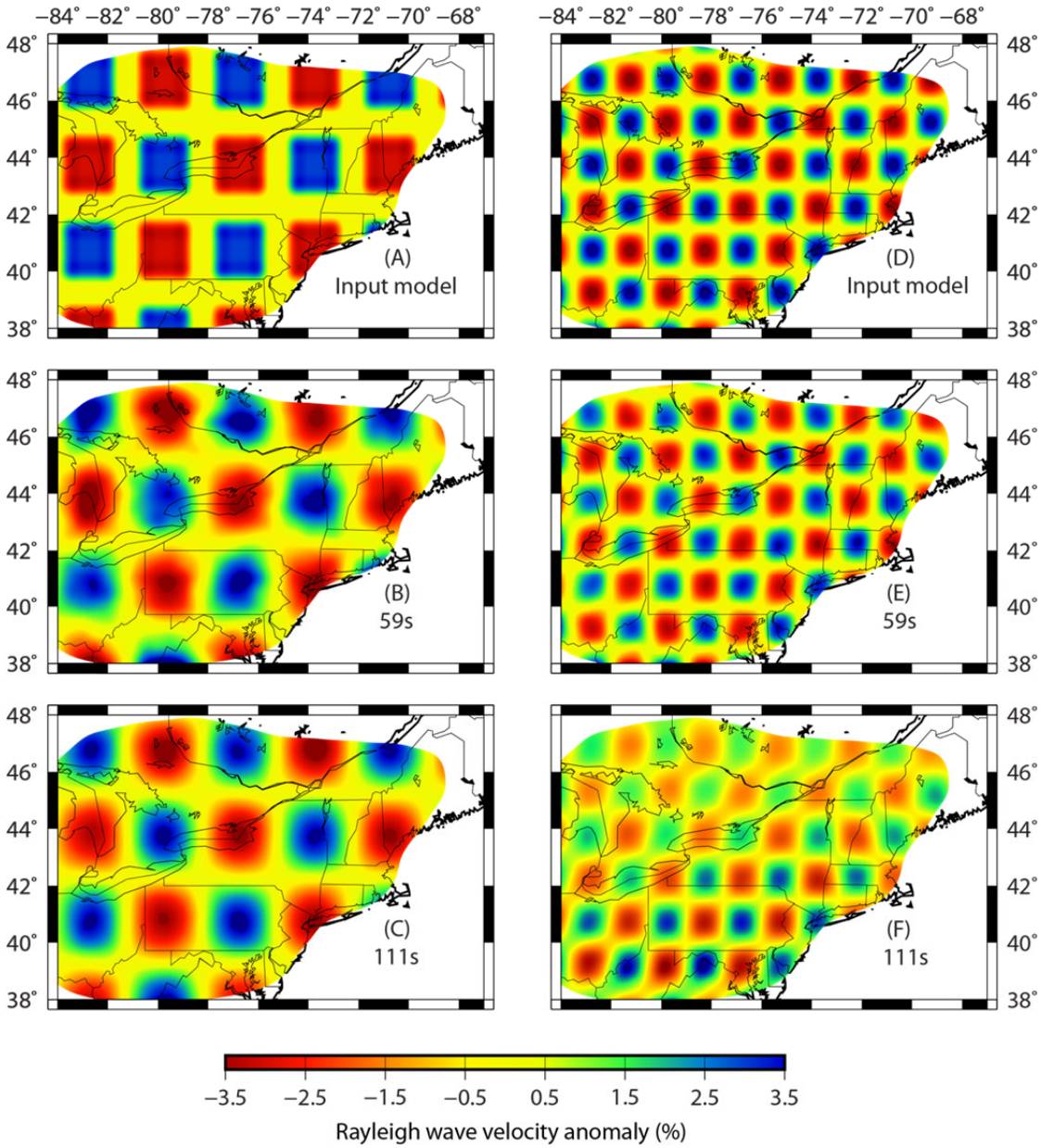

Figure S3: Resolution tests for checkerboard models from Rayleigh wave data. (A) The input model with the velocity perturbation of ±3% at a scale of 200 km by 200 km. (B-C) The recovered models at 59 s and 111 s for the input model in (A). (D) The input model with the velocity perturbation of ±3% at a scale of 50 km by 50 km. (E-F) The recovered models at 59 s and 111 s for the input model in (D).

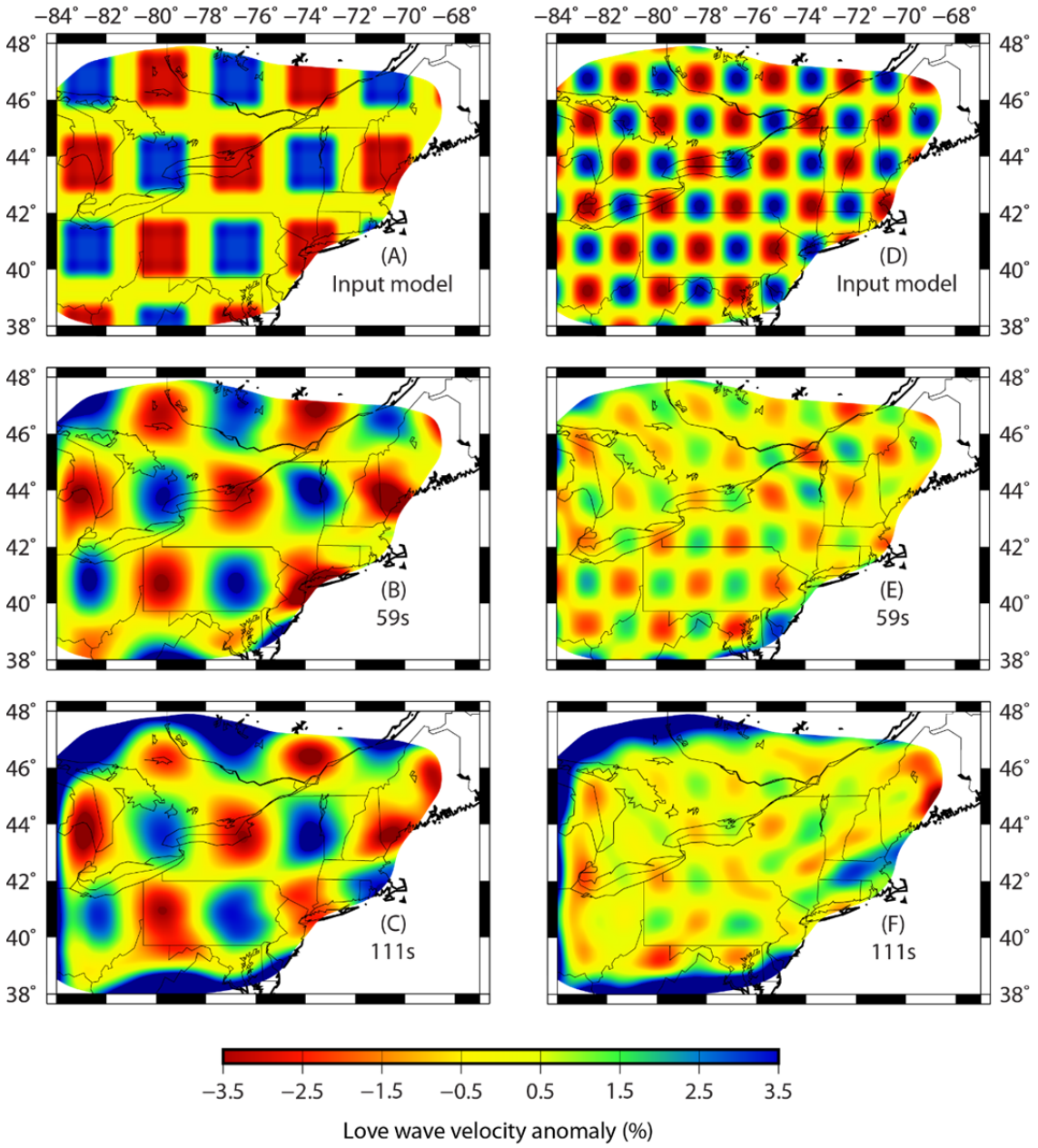

Figure S4: Resolution tests for checkerboard models from Love wave data. (A) The input model with the velocity perturbation of ±3% at a scale of 200 km by 200 km. (B-C) The recovered models at 59 s and 111 s for the input model in (A). (D) The input model with the velocity perturbation of ±3% at a scale of 50 km by 50 km. (E-F) The recovered models at 59 s and 111 s for the input model in (D).

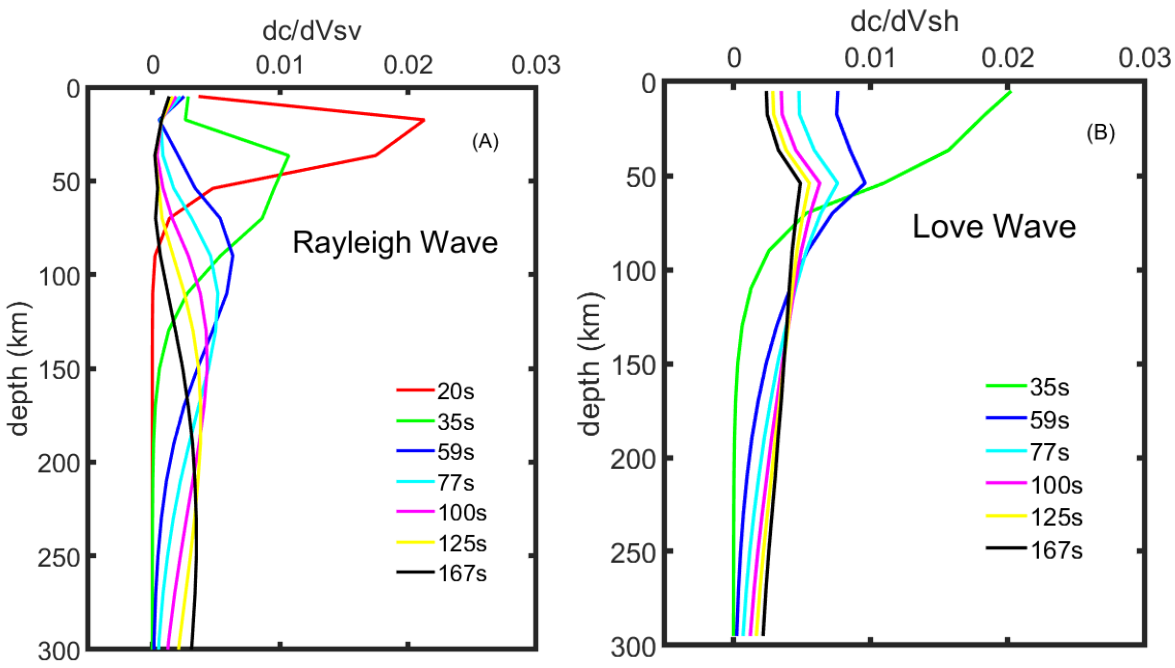

Figure S5: Sensitivity kernels of Rayleigh wave (A) and Love wave (B) from the model AK135 (Kennett et al., 1995).

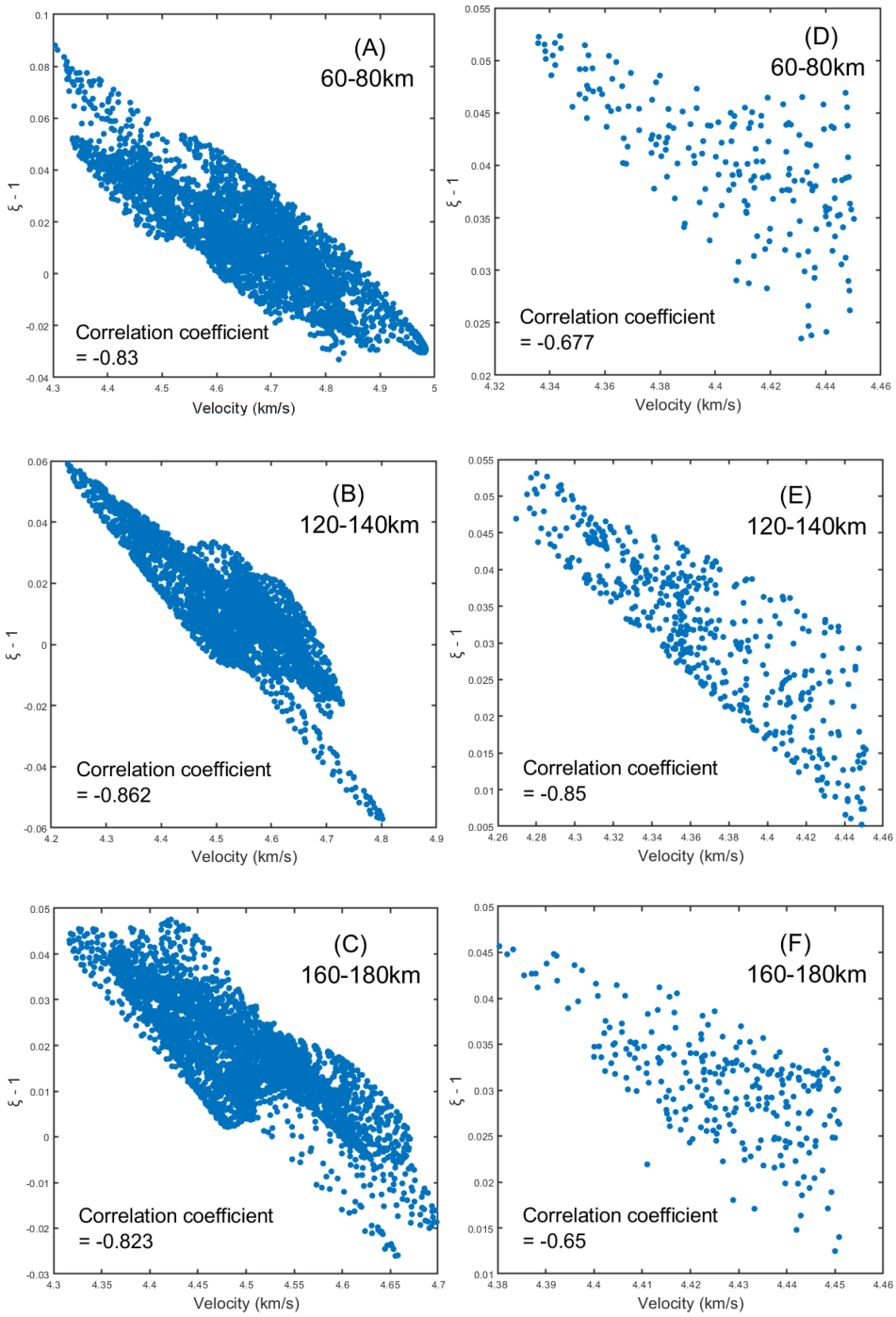

Figure S6. (A-C) Shear wave velocity versus radial anisotropy (ξ - 1) in the complete study region at different depths. (D-F) Shear wave velocity versus radial anisotropy (ξ - 1) in the low-velocity anomaly region in New England at different depths. Correlation coefficients between velocity and radial anisotropy are shown in each panel.

REFERENCES CITED

1. Kennett, B.L.N., Engdahl, E.R., and Buland, R., 1995, Constraints on seismic velocities in the Earth from travel times: Geophysical Journal International, v. 122p. 108-124.
2. Saito M., 1988, DISPER80: A subroutine package for the calculation of seismic normal mode solutions, in Doornbos D.J., ed., Seismological algorithms: Computational methods and computer programs : New York, Elsevier, p. 293–319.